

Development of an adhesive-bonded counterflow microchannel heat exchanger

Prawin Paulraj*, Brian K. Paul & Richard B. Peterson

School of Mechanical, Industrial and Manufacturing Engineering
Oregon State University
204 Rogers Hall
Corvallis, OR 97331

*Corresponding author address:

7871 SW 173rd Pl.,
Beaverton, OR 97007
Phone: 503-550-5690
Fax: 503-627-5538
E-mail: paulraj_prawin@yahoo.com

Abstract

A low-temperature liquid-to-vapor counterflow microchannel heat exchanger has been redesigned and fabricated using a scalable, low-cost adhesive bonding process. Adhesive erosion concerns are mitigated with the use of sealing bosses. Performance has been tested using water and compressed air as test fluids. Results show greater effectiveness and higher heat transfer rates than the original heat exchanger due to relaxed design constraints afforded with adhesive bonding. A maximum effectiveness of 82.5% was achieved with good agreement between theoretical and experimental values. Although thermal performance was improved, higher pressure drops were noted. Pressure drops were predicted with a maximum error of 16% between theoretical and experimental values. Much of the pressure drop was found to be in the device manifold which can be improved in subsequent designs.

Keywords: adhesive bonding, microchannel array, counterflow heat exchanger, effectiveness, pressure drop

1 Introduction

Microchannel process technology (MPT) is the use of microchannel arrays for the bulk processing of mass and energy. Although MPT devices can be on the order of meters in dimension, MPT devices include critical microchannel dimensions ranging from below 100 μm to several mm [1]. One of the major advantages of MPT is the high surface area to volume ratios compared to conventional fluidic technology. These ratios allow accelerated rates of heat and mass transfer within microchannels due to short diffusional distances. As a result, microchannels provide the ability to reduce the size and weight of a wide variety of energy and chemical systems including microelectronic cooling systems (Kawano et al. [2]; Little [3]), chemical reactors and separators (Cao et al. [4], Matson et al. [5]), fuel processors (Ryi et al. [6]), and heat pumps (Garimella et al. [7]) among many others.

A significant barrier to commercializing MPT has been the cost of manufacturing microchannel arrays [8, 9, 10]. Prior work has demonstrated and characterized a new approach to bonding low-temperature microchannel arrays that relies on mass production techniques for electronics assembly [11]. The new approach involves the use of surface mount adhesives to bond a stack of microchannel laminae (thin layers of material also referred to as shims) with

integrated height control features or sealing bosses. The objective of this paper is to demonstrate the feasibility of using this approach in the redesign of a microchannel heat exchanger, in an effort to investigate its value.

1.1. Need for Low-Temperature, Low-Cost MPT Applications

One growing area for MPT application is low-temperature thermal management, such as the cooling of consumer electronics. The peak operating temperatures for electronics cooling rarely exceeds 125°C, limited by several factors such as thermal leakage currents, ergonomics and safety. This implies that high bond strength as a function of temperature is not needed for electronics cooling and other low temperature applications such as climate control and recuperation. Thus, it can be reasoned that the commonly used bonding technique for MPT production (i.e. diffusion bonding) results in excessive process capability. A consequence of this excess process capability is the high cost of diffusion bonded devices due to an energy intensive bonding process, associated heat treatments and significant capital outlay for bonding equipment.

The adhesives mentioned in this paper are suitable for low-temperature operations ranging from -20°C to 100°C. Using custom developed adhesives, higher temperatures around 150-175° are expected to be feasible with this technique.

2 Constraints with Original Design

A stainless steel counterflow heat exchanger (liquid to vapor) with microchannel features was originally designed for a fabrication process involving photo-chemical machining (PCM) and diffusion bonding. In this study, it was redesigned to improve its manufacturability in part through the use of the adhesive bonding process. Some specifications for the two heat exchangers are outlined in Table 1.

Figure 1 shows the lamina designs for the two heat exchangers. Typically, in the design of microchannel heat exchangers, bosses (ribs or islands) can be added for any one of four purposes. First, ribs can be used to direct flow in an effort to eliminate flow maldistribution. Second, ribs and islands can be used to avoid creep, fin buckling or other failure mechanisms known to occur during diffusion bonding by distributing bonding pressure, reducing local stresses and reducing channel spans. Third, standalone features can be used to resist channel deformation during heat exchanger operation by reducing channel spans. Fourth, these features ultimately control the channel height, which is the critical dimension in microchannel arrays.

2.1. Patterning and Diffusion Bonding Constraints

Fin aspect ratios (ratio of channel span to adjacent lamina thickness; shown by w/t in figure 2) are severely restricted due to the high pressures needed during diffusion bonding. For the diffusion bonding of two-fluid microchannel devices made out of stainless steel, the critical limit established by Paul et al. [12] was 6:1 for a 500 μm thick lamina. Exceeding the critical limit resulted in unbonded fin regions at locations 1 and 2 as shown in figure 2 (top). Moreover, the critical limit was shown to decrease with increasing lamina thickness. For instance, increasing the lamina thickness to 1000 μm reduced the aspect ratio to 4:1, requiring more ribs to transmit bonding pressure. Paul et al. [12] concluded that while a thicker fin would increase the stiffness, the acceptable span does not increase linearly with thickness

due to non-linearities in plate mechanics. Consequently, geometries with higher fin aspect ratios can be hermetically sealed with diffusion bonding (at locations 1 and 2 in figure 2) when using thinner laminae. As a result, figure 1 (top-exploded header area) shows islands used in the header region (along with vertical ribs in the active region) to reduce channel spans, in order to not violate the critical aspect ratio limit during diffusion bonding.

Use of photo-chemical machining (PCM) as a patterning process constrains the geometry further. Isotropic etch limitation in PCM patterning forces an increase in the width (shorter dimension) of the islands/ribs (figure 1 exploded area) if thicker laminae are used. On the contrary, fin thickness cannot be arbitrarily reduced, due to the need to produce fluid ports and other through-features. The net result of using thicker laminae is an increase in rib/boss area due to etch constraints. This is undesirable as an increase in boss area reduces the active area in the heat exchanger. This forces a tradeoff between boss area and lamina thickness.

The combination of PCM patterning and diffusion bonding is biased towards thinner laminae due to the constraints mentioned above. As a result, the original heat exchanger design (PCM + diffusion bonding) uses two thinner laminae to form a single microchannel layer. A schematic of the design, along with the fin aspect ratio is shown in Figure 2 (top) for the diffusion-bonded heat exchanger.

2.2. Constraints due to Cooling Rates

In addition to patterning and high bonding pressures, cooling rates introduce additional constraints with diffusion bonding. In the microchannel active area (indicated by dashed lines in figure 1), fin aspect ratios are even further constrained by the cooling rates in diffusion bonding which can lead to thermal stresses large enough to warp even small aspect ratio fins [13]. Cooling rates as slow as 0.1 °C per minute have been employed to avoid these thermal stresses. With bonding temperatures over 1000 °C, this can lead to cooling times of several days. Consequently, the designer using diffusion bonding is faced with either long cycle times or small fin spans with large pressure drops and reduced active areas [14].

3 Design Considerations with Adhesive Bonding

One key lamina design feature for adhesive bonding is the need to use sealing bosses. Prior work involving the use of sealing bosses within microlamination architectures has been in conjunction with the entrapment of poly(dimethylsiloxane) (PDMS) membranes adjacent to polymeric microchannel arrays for implementing membrane microvalves [15] with compression seals. Two distinguishable functions performed by sealing bosses in adhesive bonding are: 1) to constrain the adhesive to desired locations during bonding, thereby preventing the clogging of adjacent channels; and 2) to provide a protective shroud for the adhesive during operation of the heat exchanger in an effort to minimize adhesive erosion.

Adhesive bonding uses significantly lower pressures, thereby permitting much larger aspect ratios than diffusion bonding. This allows the use of thicker laminae. The use of thicker material in the adhesive-bonded design resulted in a 50% reduction in the number of laminae as shown in Figure 2 (bottom).

In the new design, the larger aspect ratio enables the channel header area (figure 1 bottom) to be implemented without islands significantly reducing the pressure drop through the lamina. Further, because of the reduction in small island features, the adhesive-bonded lamina design

is much easier to implement using stamping, which could further reduce lamina patterning costs.

3.1. Constraints due to Operating Pressure

In addition to bonding pressures, another source of fin deflection can be differential fluid pressures on the two sides of the fin during operation. For the adhesive-bonded design, fin aspect ratios as high as 100:1 were used in the channel headers. Analysis based on a finite element model showed that the maximum deflection under operating pressures (413 kPa differential pressure) for the worst case (in channel headers, longest span) was 7%. Wattanutchariya determined that the effectiveness of stainless steel microchannel heat exchangers drops off precipitously at microchannel fin deflections beyond 10% [16]. The deflection changes the channel dimensions through the array causing flow maldistribution between channels leading to lower heat transfer performance and higher pressure drop. Fin deflection during operation is therefore a limiting factor in the adhesive-bonded design, even though higher aspect ratios can be bonded using the adhesive process.

3.2. Constraints due to Flow Uniformity

For the adhesive-bonded design, the minimum aspect ratio in the microchannel area is 14:1. Although aspect ratios as high as 100:1 could be used based on deflection modeling, the bosses (vertical ribs) are used for a different purpose here. The bosses in the adhesive-bonded design were designed to provide good flow distribution across the microchannel array. Based on a computational fluid dynamics analysis (see below) and the relaxation of bonding conditions discussed above, the number of bosses/ribs in the microchannel active area was able to be reduced from 25 to 9 (see figure 1-active area). With further analysis in flow distribution modeling, it is expected that even fewer bosses may be possible, thereby increasing the available active area.

3.3. Adhesive Bonding Design Changes

As noted earlier, the adhesive-bonded design uses thicker material resulting in the processing of 50% fewer laminae compared with the diffusion-bonded design. For the redesign, lamina 1 (used with fluid 1) is 762 μm thick with an etch depth of 254 μm . Lamina 2 is 1016 μm thick with an etch depth of 508 μm . The web of material between the fluid layers (i.e. fin thickness) remains the same at 508 μm for both designs (denoted as F in figure 2). Critical channel heights remain the same for both designs as noted in table 1. The device was designed to withstand a differential fluid pressure of 413 kPa (60 psig), with a 2.5X safety factor on adhesive bonding area.

Other significant changes for adhesive bonding also included the redesign of lamina inlet and outlet headers, the size of the device margin and the number of bosses (ribs) for distributing flow. These changes allowed an increase in the active area of the lamina. The number of bosses and the number of inlet/outlet headers was based on an optimization of flow distribution, fin deflection and active surface area within the heat exchanger. Consequently, the final number of fluid headers was increased to 7 per lamina (from 6). Under these conditions, flow analysis using a finite-volume model (Flotherm) showed velocity maldistribution (ratio of highest to lowest velocity) of approximately 12% across the microchannel active area, which was considered satisfactory from a performance standpoint.

Comparison of the two heat exchanger designs as shown in table 2 indicated the following,

- Header area increases by 22% with the adhesive bonded design. This is due to lack of islands with the new design as noted earlier. Header areas are indicated with solid lines and shown by the light and dark blue regions in figure 1.
- Active microchannel area increases by 17% with the new design. More of the device margin is used with adhesive bonding. Active areas are indicated with dashed lines and shown by the light and dark green regions in figure 1.
- The ratio of boss-to-active area increases by 19% with the new design. This indicates that the bosses (ribs) are fairly large when compared to diffusion bonding. Using thicker laminae with adhesive bonding results in wider bosses due to PCM etch constraints, as noted in section 2.1. The use of double sealing bosses also increases the inactive boss area in the adhesive bonded design. Boss areas are indicated with dotted lines and shown by the grey regions in figure 1.

However, it is expected that the new design could be further improved. The adhesive-bonded laminae were originally redesigned for stamping. Due to tooling costs, the design was converted to a PCM design. Consequently, the bend radius during stamping dictated the size of the adhesive-bonded bosses. Table 2 shows the additional savings that could be achieved by designing the laminae for PCM (optimized PCM adhesive bonded). Redesign for PCM involved reducing the size of internal bosses and eliminating the outer boss ring. With these changes, the following improvements can be achieved.

- Header area increases by 22% as before.
- Active microchannel area can be increased by 31%.
- The ratio of boss-to-active area increases by 5% over diffusion bonding.

The analysis suggests that the adhesive-bonded approach can lead to significant reductions in heat exchanger size on the order of 20 to 30% for the same heat load. The increased channel header area also suggests lower pressure drops. However, a drawback of this method is the relatively large size of the double sealing bosses when compared to diffusion bonding.

4 Theoretical Estimations of Thermal Performance

4.1. Effectiveness Calculation

If the inlet and outlet temperatures of the two fluids are known, the heat transfer rates for the hot and cold fluid can be calculated as follows,

$$Q_h = \dot{m}_h C_{p,h} (T_{h,i} - T_{h,o}) \quad (1)$$

$$Q_c = \dot{m}_c C_{p,c} (T_{c,o} - T_{c,i}) \quad (2)$$

where \dot{m}_h, \dot{m}_c are the mass flow rates, $C_{p,h}, C_{p,c}$ are the constant specific heats (assuming no phase change), and $T_{h,i}, T_{h,o}, T_{c,i}$ and $T_{c,o}$ are the inlet and outlet temperatures of the hot and cold fluids respectively.

Assuming negligible heat transfer rates to the ambient and negligible potential and kinetic energy changes for both fluids, an energy balance may be computed as

$$Q_h = Q_c \rightarrow \dot{m}_h C_{p,h} (T_{h,i} - T_{h,o}) = \dot{m}_c C_{p,c} (T_{c,o} - T_{c,i}) \quad (3)$$

The effectiveness of a heat exchanger relates the effective heat transfer rate to the maximum transfer rate, or

$$\varepsilon = \frac{Q}{Q_{\max}} \quad (4)$$

where Q and Q_{\max} are the effective and maximum transfer rates of the device. The experimental effectiveness can be simplified to a temperature difference ratio as follows,

$$\varepsilon = \left(\frac{T_{c,o} - T_{c,i}}{T_{h,i} - T_{c,i}} \right) = \left(\frac{T_{h,i} - T_{h,o}}{T_{h,i} - T_{c,i}} \right) \quad (5)$$

Heat exchanger effectiveness can also be predicted using theoretical analysis as below

The overall heat transfer coefficient (U) can be related to the respective heat transfer coefficients between the two sides using the Wilson plot [17] method as follows,

$$1/U = 1/h_h + t_w / \lambda_w + 1/h_c \quad (6)$$

where t_w and λ_w are the thickness of the partition wall and thermal conductivity of the wall material, h_h and h_c are heat transfer coefficients of the hot and cold fluid respectively.

The Nusselt number (Nu) is defined as

$$Nu = \frac{hD_h}{\lambda} \quad (7)$$

where D_h is the hydraulic diameter of the microchannel passage. The Nusselt number is constant for fully developed, laminar flow (6.99 for a rectangular microchannel with an aspect ratio of 14 using constant temperature condition). For this study, the Reynolds number for the airflow side varied from 295 to 2060 indicating laminar flow. For the full-scale device projections, fluidic property differences (R245fa) such as density and viscosity account for slightly higher Reynolds numbers as shown in table 3. However, it is noted that the flow is much closer to laminar flow regime than turbulent regime. Laminar flow analysis is therefore considered to be appropriate for the full-scale devices.

For a counterflow heat exchanger, the theoretical effectiveness can be obtained using the number of transfer units (NTU) and heat capacity ratio (C_R) using the following relationship [18],

$$\varepsilon = \frac{1 - \exp[-NTU \cdot (1 - C_R)]}{1 - C_R \cdot \exp[-NTU \cdot (1 - C_R)]} \quad (8)$$

where NTU and C_R are defined as

$$NTU = \frac{UA}{(\dot{m}Cp)_{\min}} = \frac{UA}{C_{\min}} \quad (9)$$

$$C_R = \frac{(\dot{m}Cp)_{\min}}{(\dot{m}Cp)_{\max}} = \frac{C_{\min}}{C_{\max}} \quad (10)$$

where A is the area of the heat exchanger and C_{\min} and C_{\max} are the heat capacity rates of the two fluids.

4.2. Pressure Drop Calculation

The total (system) pressure drop in a heat exchanger can be calculated as the sum of major and minor losses. Major losses are friction losses, while minor losses occur due to geometry of the system (valves, bends, expansion and contraction).

Using the Darcy-Weisbach equation for fully-developed flow, friction loss in a section is expressed as follows

$$\Delta p_{major} = f \cdot \frac{L}{D_h} \cdot \frac{\rho V^2}{2} \quad (11)$$

where L, D_h and V is the length, hydraulic diameter and average fluid velocity in the section, ρ is the density of the fluid and f is the friction factor.

For laminar flow, the Darcy friction factor is a function of Reynolds number (Re) as follows,

$$f = \frac{64}{Re} \quad (12)$$

Friction factor for turbulent flow is obtained from Moody diagram using Reynolds number (Re) and relative roughness (ϵ/D ratio of mean roughness to pipe diameter). Turbulent flow was noted in the inlet and outlet tubes of the fluid manifolds (SS 316L; $\epsilon/D = 0.00025$).

Minor losses are computed as follows,

$$\Delta p_{minor} = K_L \cdot \frac{\rho V^2}{2} \quad (13)$$

Where K_L is the loss coefficient associated with a particular geometry.

The total pressure drop constitutes the sum of the major and minor loss components,

$$\Delta p_{Total} = \sum_1^n \Delta p_{major} + \sum_1^x \Delta p_{minor} \quad (14)$$

5 Experimental Approach

5.1. Test Article

Due to test setup limitations, a partial heat exchanger (Figure 3) was built from two laminae; one for each fluid. Based on the adhesive bonding process described in [11], sealing bosses were patterned on laminae (Stainless Steel 316L) using PCM. A controlled amount of adhesive (Loctite 3621) was deposited between the sealing bosses using a dispenser (Asymtek Spectrum S-820). Laminae with adhesive were stacked on top of each other and cured at low temperatures ($<150^{\circ}\text{C}$) to produce the bonded device. Characterization of typical bonds and cross-sections are described in detail elsewhere [11].

5.2. Experimental Setup

The 2-layer microchannel heat exchanger was installed in a test loop to evaluate thermal and pressure drop performance. Fluid manifolds were attached to the heat exchanger using an epoxy adhesive (J-B Weld). The test device was covered in foam insulation and plastic hoses were attached using clamps. Hot water (fluid 1 used with lamina 1-762 μm) and compressed air (fluid 2 used with lamina 2-1016 μm) were used as the working fluids. For pressure drop testing, the airflow was varied from 150-1100 cm^3/s (20-140 CFH). For effectiveness testing, water flow was maintained at 0.32 cm^3/s (0.3 GPH) and airflow was varied from 150-1100 cm^3/s (20-140 CFH). Inlet and exit pressures were measured for both fluids using pressure transducers (Omega DPG1000b-15G) and temperatures were measured using K-type thermocouples. Flow rate was measured using flowmeters for both water and airflow. Flow rate uncertainties were estimated at 0.014 cm^3/s (0.013 GPH) for water flow and 19.7 cm^3/s (2.5 CFH) for air flow respectively. The uncertainty in the pressure transducers was 0.034 kPa and temperature measurement uncertainty was 0.05 $^{\circ}\text{C}$. The maximum errors in pressure drop and effectiveness were estimated at 6% and 2% respectively.

6 Results and Discussion

6.1. Experimental Effectiveness

The experimental and estimated values of heat exchanger effectiveness are compared in Figure 4. The predicted values exclude axial conduction losses and show that the theoretical effectiveness varies from roughly 0.99 to 0.55, decreasing with increasing airflow rates. This effect is clearly explained by equations 8 and 10. The effectiveness decreases as the capacity rates of the two fluid streams approach each other. The experimental effectiveness varies from 0.825 to 0.55. At very low airflow rates, the difference between the theoretical and experimental values is quite large. The energy balance errors for the three lowest airflow settings were 48%, 27% and 17% respectively, indicating that heat loss was significant. Sources of heat loss include axial conduction and leaks to ambient. Energy balance errors for the remaining airflow settings were less than 5%, indicating that axial conduction dominated at low flow rates and was relatively unimportant at higher flow rates.

6.2. Effectiveness-Full Scale Extrapolation

Using the theoretical analysis as described in section 4.1, results extrapolated to the two full-scale designs are shown in table 3. R245fa liquid (fluid 1 used with lamina 1; 254 μm channel height) and R245fa vapor (fluid 2 used with lamina 2; 508 μm channel height) are used as fluids for the two full-scale devices. The full-scale devices have a total of 65 fluid layers (32 fluid 1 layers +33 fluid 2 layers). From table 3, it is noted that the Reynolds numbers for the full-scale devices are 2320 and 2720 respectively, for the diffusion and adhesive bonded designs. As mentioned earlier, laminar analysis is still considered appropriate as the flow regime is much closer to laminar than turbulent flow.

For the full-scale device comparison, available heat exchanger area increases by 17% in the new design (see section 3.3) as noted in table 2, resulting in a corresponding increase in NTU. A greater effectiveness (+4%) and larger heat load (+6%) is realized in the new design as a result of the increase in NTU. Using an optimized PCM adhesive bonded device, NTU increases by 31%, resulting in a 7% increase in effectiveness and 11% increase in heat load. Regardless of optimization, the implication is that a smaller heat exchanger is possible with the adhesive-bonded design providing additional raw material savings.

6.3. Experimental Pressure Drop

In figure 5 (top), the theoretically calculated system (total) pressure drops for the test device are compared with experimental data for the airflow side. The system pressure drop includes losses when the fluid enters the inlet manifold and exits the outlet manifold, and is schematically shown in figure 5 (bottom). The experimental pressure drop varies approximately with the square of the flow rate, and is expressed with a least squares fit as shown in the figure 5 (top). Experimental results are in excellent agreement with pressure drop calculations as shown in section 4.2. The maximum variation between the experimental and theoretical values is 16%, with the maximum pressure drop of 28.3 kPa at the highest flow rate.

6.4. Pressure Drop-Full Scale Extrapolation

Since the manifold details were unknown for the diffusion-bonded device, the pressure drop across a single lamina was calculated for both designs and compared in Table 3. The adhesive-bonded design has approximately 42% higher pressure drop (9.4 kPa) than the diffusion-bonded design (6.6 kPa). The adhesive-bonded design has approximately 14% higher average fluid velocity in the microchannel section due to fewer, albeit larger flow passages.

In comparing table 3 and figure 5, it is apparent that the single lamina pressure drop (9.4kPa) is approximately 3X lower than the experimentally measured system pressure drop of 28.3kPa. A breakdown of the pressure loss components (figure 5 bottom) indicates that the total pressure loss across a single lamina is approximately 27% (dotted region in figure 5 bottom), while other (non-lamina) losses (friction loss in manifold tubes + minor losses) are fairly large at 73%. A redesign of the manifolds (circled region in figure 5 bottom) would significantly reduce minor losses due to expansion and contraction. For example, doubling the diameter of the inlet and outlet tubes reduces non-lamina losses to 32% of system pressure drop.

6.5. Erosion mitigation in adhesive bonding

Metallic microchannel coolers used for laser-diodes have experienced reliability issues due to erosion of microchannels [19, 20]. High water velocities cause erosion due to presence of particles in the process cooling water. Rapid erosion of adhesive bonds is therefore a serious concern that needs to be addressed with the proposed method. The sealing bosses used to constrain the adhesive also provide a protective shroud acting as a barrier separating the adhesive from the fluid. The bosses do not provide a water-tight seal but have a small gap that has been characterized elsewhere [11]. While the gap provides fluidic access to the adhesive, the pressure drop across the gap is very large, significantly reducing the velocity of the water that impacts the adhesive. Flow simulations show a 45-65X reduction in velocity components under an experimentally characterized gap of 15 μ m [11]. Using erosion models developed by Oka et al. [21, 22], the adhesive is expected to erode at about 1/7th the rate of stainless steel base material at the worst-case wall gap. Using a measured wall gap of 15 μ m, the adhesive erodes at a remarkable 515X slower than stainless steel base metal. This implies that the adhesive bond will outlast the metallic base material and requires that the device be taken out of service prior to complete base metal erosion.

7 Conclusions

An adhesive-bonded, air-water microchannel counterflow heat exchanger has been designed, fabricated and tested, and shown to provide improved heat transfer performance for air flow rates up to 1100 cm³/s (140CFH). Relaxed aspect ratios resulted in 50% reduction in the number of laminae in the new design. Results suggest a 31% increase in active area for a given footprint using optimized PCM and adhesive-bonded design. A maximum effectiveness of 82.5% was achieved with good agreement between theoretical and experimental values at high flow rates. The new design has a larger NTU due to a 17% increase in active area, resulting in a higher effectiveness and greater heat dissipation within the same footprint. This suggests that a smaller heat exchanger is possible with the adhesive-bonded design, implying additional savings. The penalty for improved heat transfer is a higher pressure drop than the original design due to fewer flow passages in the microchannel section. Air-side experimental pressure drops were in good agreement with theoretically predicted pressure drops. High experimental pressure drops can be lowered by increasing the diameter of the inlet and outlet headers ensuring that the full-scale device meets pressure drop specifications. Flow simulations and erosion calculations indicate that the base metal erodes much more rapidly than the adhesive bonds eliminating concerns about adhesive erosion.

8 Acknowledgements

The authors would like to thank Dr. Hailei Wang for experimental layout and thermal consultations, and Kevin Harada for help in test loop setup.

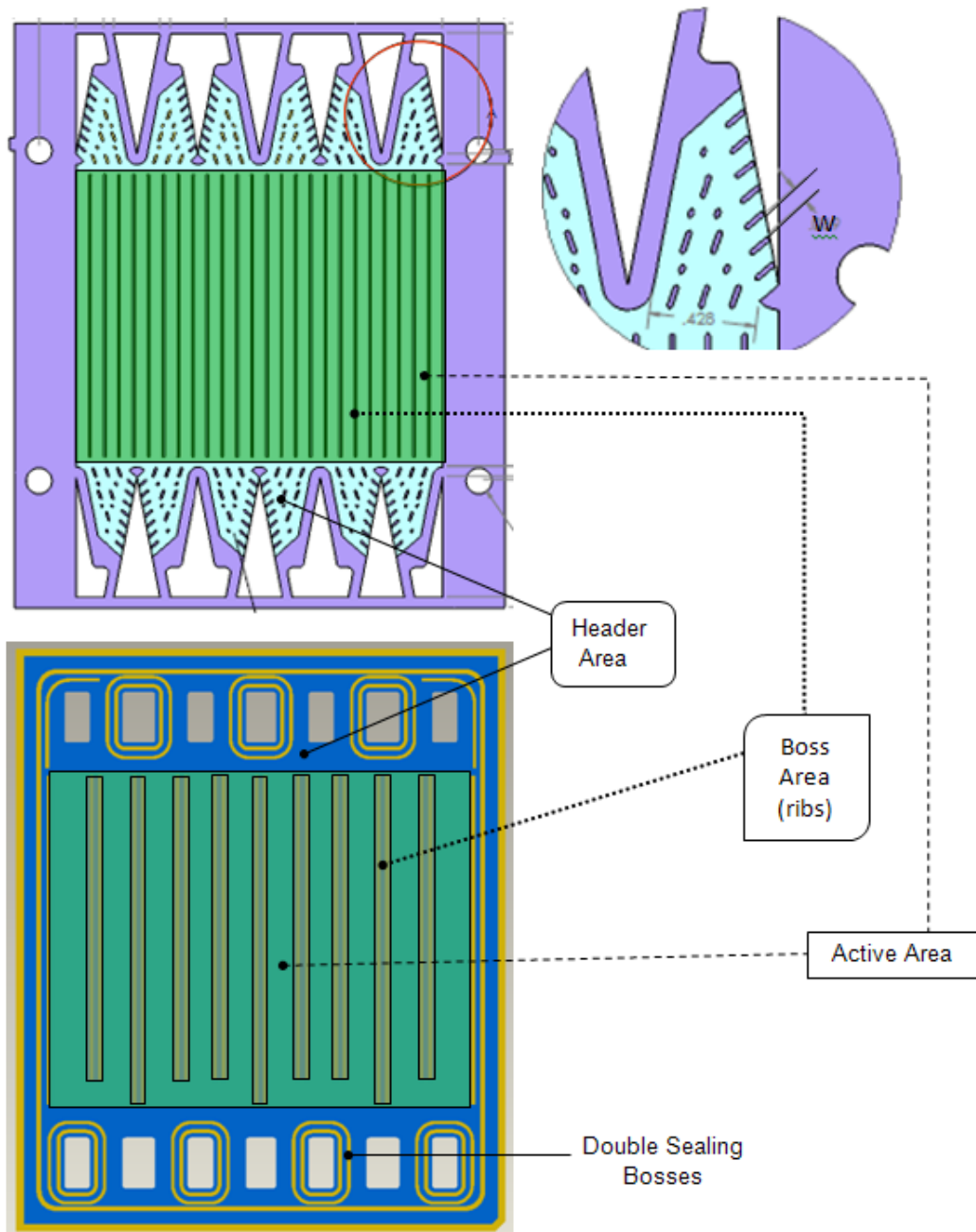


Figure 1: Comparison of lamina designs between diffusion (top) and adhesive bonding (bottom). The top exploded area shows islands in the header region. Notice the lack of islands and fewer bosses/ribs in the adhesive design. Header, boss and active areas are shown in the two designs.

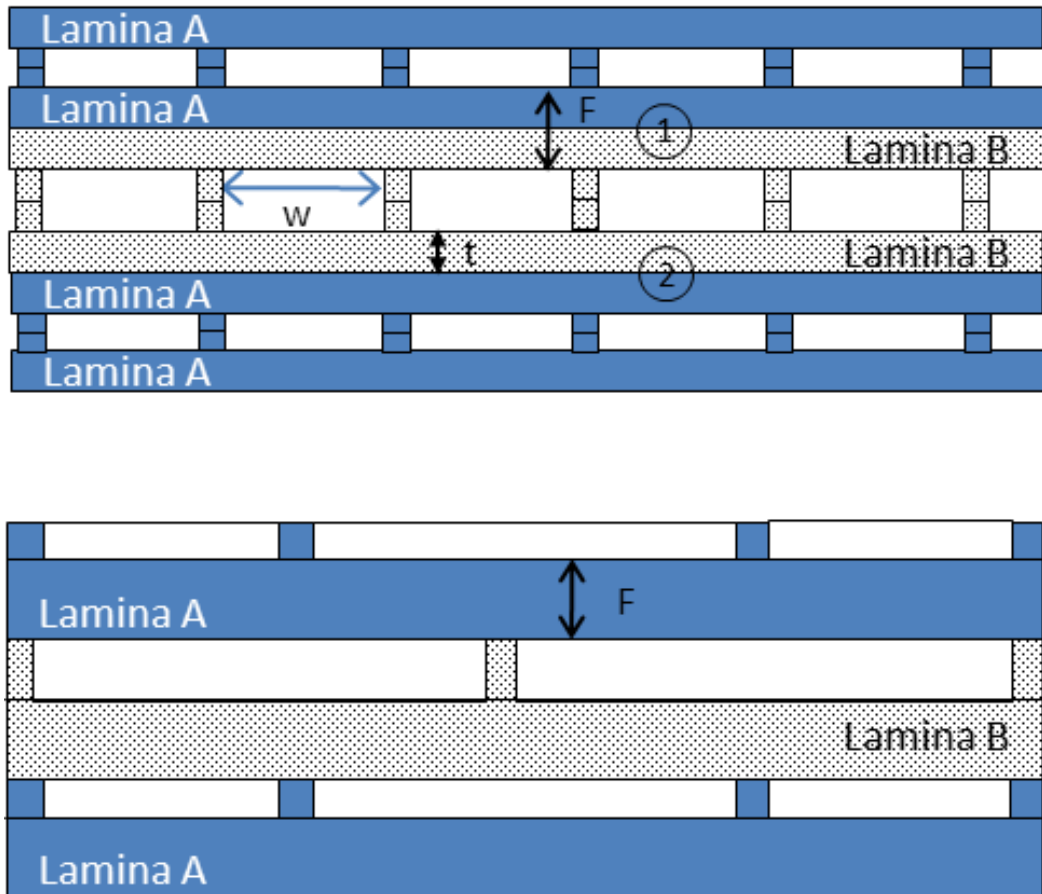


Figure 2: Lamina design comparison. Diffusion-bonded design is shown on top. Fin aspect ratio is defined as w/t in the above figure. Exceeding the critical aspect ratio results in unbonded fin regions at locations 1 & 2. Notice the larger channel aspect ratio in the adhesive-bonded design (bottom). This allows the new design to use 50% fewer laminae. The total fin thickness (F) remains the same in both designs.

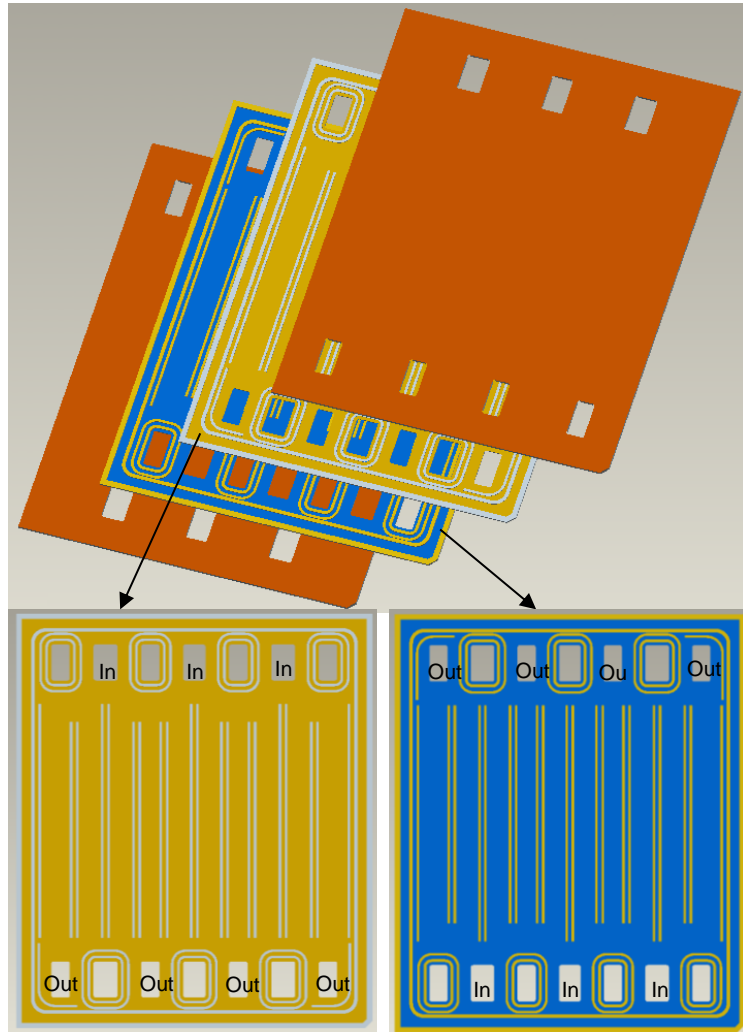


Figure 3: Schematic of 2-layer microchannel heat exchanger test device. The individual lamina designs (Lamina 1-right) and Lamina 2 (left) are also shown.

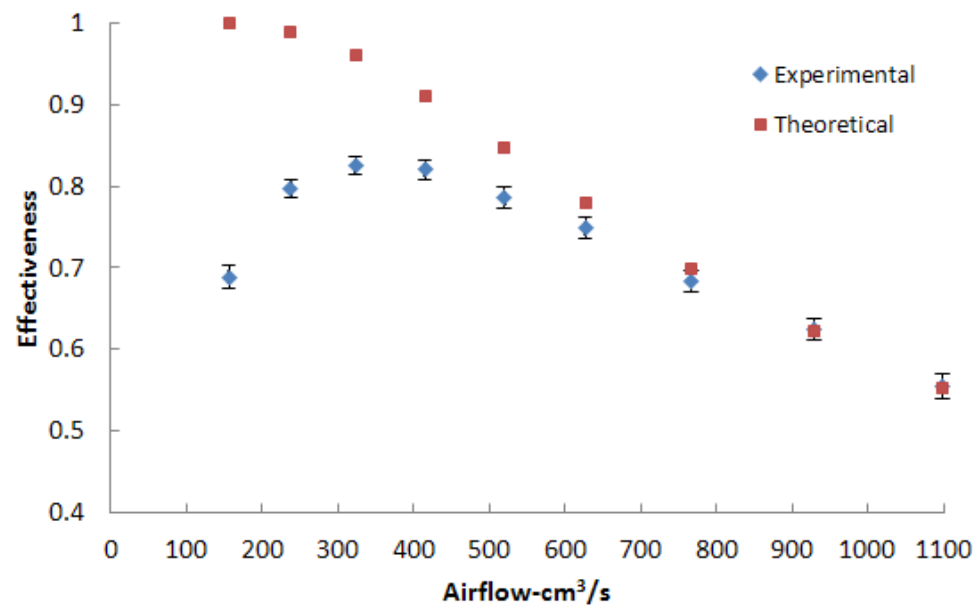


Figure 4: Comparison of experimental and theoretically calculated heat exchanger effectiveness as a function of flow rate.

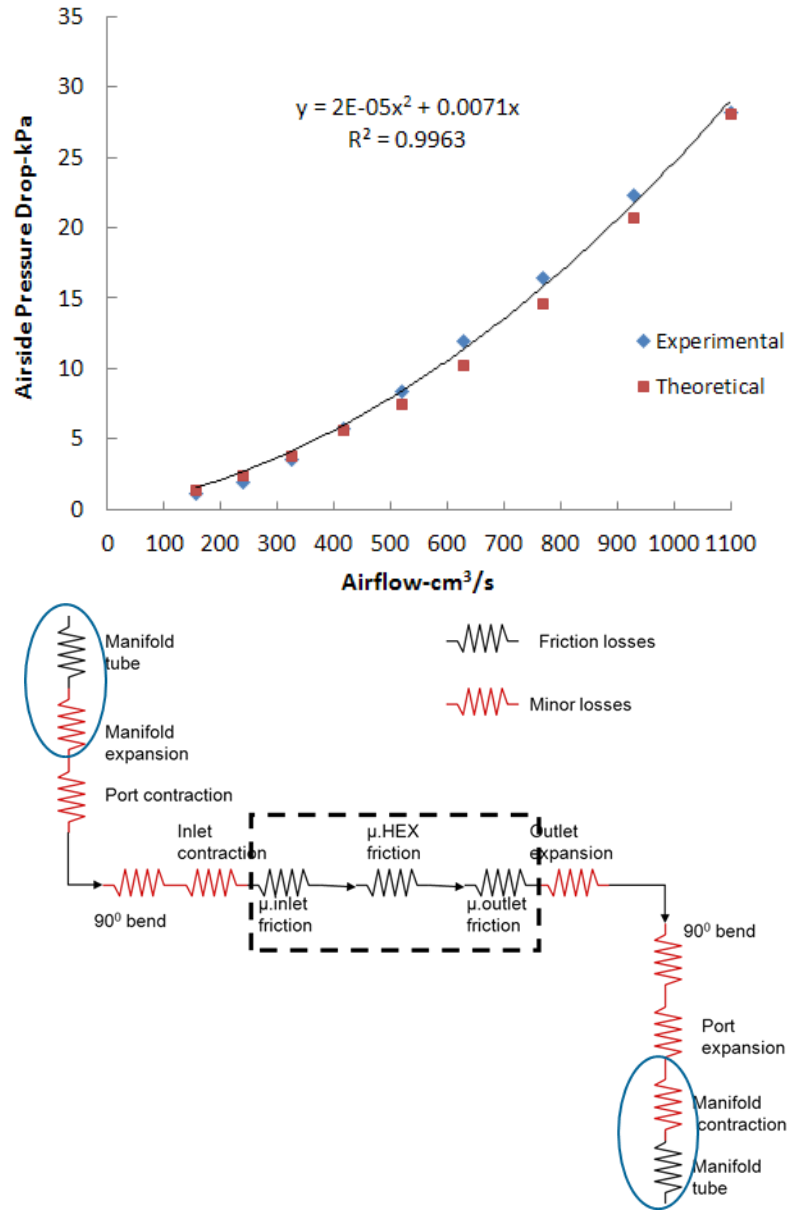


Figure 5: Comparison of experimental and calculated pressure drops as a function of airflow (top). System pressure drop components are shown below.

Table 1: Heat exchanger specifications and comparison with adhesive-bonded design.

Microchannel Heat Exchanger	Diffusion-bonded design		Adhesive-bonded design (extrapolated)	
	Fluid 1 R245fa liquid	Fluid 2 R245fa vapor	Fluid 1 R245fa liquid	Fluid 2 R245fa vapor
Number of fluid layers	32	33	32	33
Number of lamina	64	66	32	33
Mass flow rate (kg/min)	1.8	1.8	1.8	1.8
Lamina thickness (μm)	381	508	762	1016
Etch depth (μm)	127	254	254	508
Critical channel height (μm)	254	508	254	508
Fin thickness (μm)	508	508	508	508

Table 2: Comparison of heat exchanger areas between diffusion and adhesive-bonded designs.

Design	Lamina Area m ²	Active Area m ²	Boss Area m ²	Header Area m ²	Boss/Active Area Ratio %	Active/Lamina Area Ratio %
PCM/Diffusion-bonded	0.01786	0.00594	0.00096	0.00143	16.16	66.53
PCM/Adhesive-bonded (stamp simulated)	0.01786	0.00698 (+17%)	0.00247	0.00174 (+22%)	35.37 (+19%)	78.22 (+12%)
Optimized PCM/Adhesive-bonded	0.01786	0.00777 (+31%)	0.00165	0.00174 (+22%)	21.24 (+5%)	87.03 (+21%)

Table 3: Comparison of heat exchanger parameters between diffusion and adhesive-bonded designs. Results are extrapolated for full-scale devices with both designs.

Microchannel Heat Exchanger	Diffusion bonded design		Adhesive bonded design	
	Fluid 1 R245fa liquid	Fluid 2 R245fa vapor	Fluid 1 R245fa liquid	Fluid 2 R245fa vapor
Reynolds Number	81	2320	98	2720
Convection Coefficient (W/m^2K)	1340	117	1340	117
Inlet temperature ($^{\circ}C$)	51.6	16.1	51.6	16.1
Estimated outlet temperature ($^{\circ}C$)	36.3	39.8	35.3	41.4
Inlet Pressure (kPa)	517	102	517	102
Estimated pressure drop (kPa)	0.031	6.6	0.044	9.4
Heat exchanger area (m^2)		0.386		0.45
Overall heat transfer coeff. (W/m^2K)		107		107
No. of transfer units (NTU)		1.53		1.78
Effectiveness %		67		71
Heat Load (W)		643		684

9 References

- [1] Paul B.K., *Micro Energy and Chemical Systems and Multi-scale Fabrication*, Springer-Verlag, Germany, 2005, Chapter 14.
- [2] Kawano K., Minakami K., Iwasaki H., Ishizuka M., *Micro Channel Heat Exchanger for Cooling Electrical Equipment*, ASME (HTD) – Proc. ASME Heat Transfer Division, 1998, 361-3: pp. 173-180.
- [3] Little W. A., *Microminiature Refrigerators for Joule-Thomson Cooling of Electronic Chips and Devices*, *Advances in Cryogenic Eng.*, 1990, Vol. 35, pp 1325-1333.
- [4] Cao H., Chen G., Yuan Q., *Testing and design of a microchannel heat exchanger with multiple plates*, *Ind. Eng. Chem. Res.*, 2009, 48, pp. 4535-4541.
- [5] Matson D. W., et al., *Fabrication of microchannel chemical reactors using a metal lamination process*, 3rd Int. Conf. Microreaction Tech. 1999, pp. 1-11.
- [6] Ryi S.K., Park J.S., Cho S.H., Kim S.H., *Fast start-up of microchannel fuel processor integrated with an ignited for hydrogen combustion*, *J. Power Sources*, 2006, Vol. 161(2), pp. 1234-1240.
- [7] Garimella S., Determan M.D., Meacham J.M., Lee S., Ernst, T.C., *Microchannel component technology for system-wide application in ammonia/water absorption heat pumps*, *Int. J. Refrig.*, 2011, vol. 34(5), pp. 1184-1196.
- [8] Porter J.D., Paul B.K., Ryuh B., *Cost Drivers in Microlamination based on a High-Volume Production System Design*, ASME IMECE proc., Nov. 2002, pp. 267-274.
- [9] Lajevardi B., Leith S.D., King D.A., Paul B.K., *Arrayed Microchannel Manufacturing Costs for an Auxiliary Power Unit Heat Exchanger*, Proc. Ind. Eng. Res. Conf., May 2011, Reno, NV.
- [10] Leith S.D., King D.A., Paul B.K., *Toward Low-Cost Fabrication of Microchannel Process Technologies – Cost Modeling for Manufacturing Development*, Proc. 2010 AIChE Annual Meet., Salt Lake City, UT.
- [11] Paulraj P., Paul B.K., *Metal microchannel lamination using surface mount adhesives for low-temperature heat exchangers*, *J Manuf. Proc.*, 2011, Vol. 13(2), pp. 85-95.
- [12] Paul B.K., Kwon P., Subramanian R., *Understanding limits on fin aspect ratios in counterflow microchannel arrays produced by diffusion bonding*, *J. Mfg Sci. Engr*, 2006, 128(4), pp. 977-983.
- [13] Lingam G.K., Paul B.K., *Modeling of Microchannel Buckling due to Thermal Stresses during Diffusion Bonding*, *Trans. NAMRI*, 2010, Vol. 38, pp. 539-545.
- [14] Lingam G.K., Paul B.K., *Cooling Rate Limitations in the Diffusion Bonding of Microchannel Arrays*, Proc. NAMRI/SME, 2011, Vol. 39, Paper NAMRC39-4792, Corvallis, OR.

- [15] Paul B.K., Abhinkar B.S., Lee S., High pressure hermetic compression seals for embedding elastomeric membrane microvalves in polymer microfluidic devices, *Prec. Eng.*, 2011, Vol. 35(2), pp. 348-354.
- [16] Wattanutchariya W., Application of Buckling Behavior to Evaluate and Control Shape Variation in High-Temperature Microlamination, Ph.D. Thesis, Oregon State University, Oregon, 2002.
- [17] Wilson E.E., A basis for rational design of heat transfer apparatus, *Trans. ASME* 1915, Vol. 37, pp. 47-82.
- [18] Incropera F.P., DeWitt D.P., Bergman T. L., Lavine A.S., *Fundamentals of heat and mass transfer*, 6th ed. Wiley, 2006, p.389.
- [19] Haake J.M., Faircloth B., Requirements for long life micro-channel coolers for direct diode laser systems, *Proc. SPIE*, 2005, Vol.5711, pp 121-131.
- [20] Ebert T., Pajunk M., Mueller D., Priesterath W., New generation of corrosion-resistant microcoolers, *Proc. SPIE*, 2005, Vol.5711, pp 152-157.
- [21] Oka Y.I., Ohnogi H., Hosokawa T., Matsumura M., The impact angle dependence of erosion damage caused by solid particle impact, *J. Wear*, 1997, 203-204, pp 573-579.
- [22] Oka Y.I., Okamura K., Yoshida T., Practical estimation of erosion damage caused by solid particle impact Part1: Effects of impact parameters on a predictive equation, *J. Wear* 259, 2005a, pp. 95-101.